LASER INTERFEROMETER GRAVITATIONAL WAVE OBSERVATORY
- LIGO -
CALIFORNIA INSTITUTE OF TECHNOLOGY
MASSACHUSETTS INSTITUTE OF TECHNOLOGY

Publication	**LIGO-P1900188–v2**	2019/09/28

Optical Cavity Inference Techniques for Low Noise Interferometry

Jorge Ramirez
Mentors: Craig Cahillane, Anchal Gupta, Rana Adhikari

Distribution of this document:

AIC, ISC

California Institute of Technology
LIGO Project, MS 18-34
Pasadena, CA 91125
Phone (626) 395-2129
Fax (626) 304-9834
E-mail: info@ligo.caltech.edu

Massachusetts Institute of Technology
LIGO Project, Room NW22-295
Cambridge, MA 02139
Phone (617) 253-4824
Fax (617) 253-7014
E-mail: info@ligo.mit.edu

LIGO Hanford Observatory
Route 10, Mile Marker 2
Richland, WA 99352
Phone (509) 372-8106
Fax (509) 372-8137
E-mail: info@ligo.caltech.edu

LIGO Livingston Observatory
19100 LIGO Lane
Livingston, LA 70754
Phone (225) 686-3100
Fax (225) 686-7189
E-mail: info@ligo.caltech.edu

http://www.ligo.caltech.edu/

Abstract

Gravitational waves are being detected more and more frequently by the Advanced LIGO interferometers due to the improvements made to their precision. To improve the rate at which we detect gravitational waves, one method would be to reduce the noise that is intrinsic to these signals, so that more signals can be extracted with confidence. To achieve this, a deeper understanding of the noise couplings that mask these signals is necessary. This project seeks to develop statistically rigorous methods of analyzing signals from Fabry-Perot cavities and recovering otherwise difficult to measure parameters which govern these noise couplings using interferometer modeling software and Bayesian inference techniques.

1 Introduction

Gravitational waves exist as a consequence of general relativity imposing a universal speed limit on the diffusion of information in the universe. Gravitational waves cause regions of space to shrink and expand in specific directions, and any masses in this region of space will shrink and expand accordingly. This affect that gravitational waves have on spacetime is quantized in terms of the strain that occurs in any mass located in that system. The usefulness of being able to detect gravitational waves is apparent when reviewing the sources of gravitational waves and their ability to propagate. Current observational astronomy is conducted through the measurement of electromagnetic waves of varying wavelengths. Gravitational waves are an entirely different class of physical phenomenon that can be analyzed to learn more about the universe. The two main drawbacks of observing electromagnetic waves is that their energies fall off as an inverse square law. Gravitational waves are unique in that although their energy falls off as an inverse square law, the strain they induce in detectors falls off only as an inverse law. This property has profound implications for the field of observational astronomy- an upgrade that increases the sensitivity of an electromagnetic detector by 100 times will increase its range by 10, whereas the same upgrade made to a gravitational wave detector will have its range increase 100 times. [1, 2]

The strain is expressed, by convention, as the relative change in length as a fraction of the original length. For example, a 1.0 meter by 2.0 meter rectangle with an incident gravitational wave perpendicular to the norm with a strain = 0.1 will oscillate between having one side of 0.9 meters and 1.1 meters and the other side 1.8 meters and 2.2 meters. This shrinking and expanding of masses is capable of doing work as posited by the "sticky bead argument" [3], which describes a stationary rod with beads that has an incident gravitational wave induce an oscillatory strain that in turn also induces friction between the beads. Thus, it can be said that gravitational waves also carry energy and do work on systems of masses via the gravitational force. This oscillation will have sinusoidal components that correspond to the frequency of the incident gravitational wave. In addition to the strain, gravitational waves also have a period and frequency associated with their wave-like nature. These properties are inherent to the system from which they are radiated from; a binary system of supermassive black holes radiate gravitational waves with a frequency of 10^{-8} to 10^{-2} Hz, objects captured by those same black holes can radiate gravitational waves of 10^{-5} to 10^{-1} Hz, binary systems of regular black holes can radiate gravitational waves from 10^{-3} to 10^{3} Hz, and rotating non-

spherical neutron stars and non-symmetric supernovae [4].

Gravitational wave detectors have been prototyped in various forms since the 1970's by famous scientists such as Joseph Weber and Rainer Weiss [5]. The most successful detectors today belong to the LIGO Scientific Collaboration and employ laser interferometers to detect gravitational waves that pass through the earth by clever measurements of the strain induced on two perpendicular long laser beams. With these detectors, and upgrades being made to their sensitivity and noise reduction, gravitational waves are being detected more consistently than ever before. The current goal for all of these gravitational wave detectors is to improve the quality of signals that we extract from our data. This can be accomplished, broadly speaking, in two major ways: we can either improve the quality and precision of our mirrors, detector optics, and laser source inside the interferometer, or we can develop better control systems and noise reduction and filtering systems that can actively deal with the background noise. The background noise associated with gravitational waves detected by these laser interferometer detectors is a thorough blend of many different unrelated noise sources. Some of these noise sources are: *seismic noise*, environmental noise like cars or earthquakes, *thermal noise*, microscopic fluctuations of the individual atoms of the detector, *shot noise*, the quantum effect of the discrete nature of photons at the detector's photodetectors limiting their accuracy, and *laser noise*, which is noise originating from the variations in the laser's intensity and frequency.

2 Motivations

This project sought to understand the noise coupling mechanisms that allow various noise sources to "leak" into the gravitational wave signals being detected at the LIGO interferometers. In order to understand these noise coupling mechanisms, there exists a need to develop statistical methods of determining which detector parameters influence these coupling mechanisms the most, and with what confidence we can say that they do. The benefit of doing this is clear, if we can understand how noise couples to our gravitational wave signals, then work can be done to improve our control systems to counteract those specific coupling mechanisms.

In preparation for developing cavity inferencing techniques, considerable effort was placed on understanding how Fabry-Perot cavities operate. Since there are many different parameters involved at various stages of the usage of these cavities, a need for being able to corroborate analytic estimations with well-known results was established. Thus, this project employed the usage of a cavity simulation software known as `FINESSE` [6] in order to corroborate the project's analytic findings with computer numerical simulations, providing a "baseline" for the calculations done. Another advantage of the computer simulation is that there are several parameters that are either difficult, or outright impossible, to measure or tune precisely in a laboratory setting. For example, there is no way to sample the strength of the electric field of a laser at any point in a cavity (or anywhere else) since amplitude detectors do not exist. Scientists working with interferometers must work in terms of laser power by counting photons with photodiodes which introduces a new source of signal noise on the quantum level called photon shot noise.

Before being able to draw inferences from data and extract information about cavity parameters, a thorough analysis of the physics and mathematics of two mirror cavities was done in preparation for this project. The frequency domain equations which describe the strength of the electric field reflected from the cavity, the fields circulating in the cavity, and the fields transmitted through the cavity were derived and confirmed within error using the numerical simulation. They then served as a baseline for simulating how a cavity behaves as certain parameters were shifted, such as reflectivity of the incident and end mirrors, the relative microscopic distance between the mirrors, the power and frequency of the cavity laser, and finally the depth and frequency of modulation used in determining a self-correcting error signal.

After developing a simulation framework for cavities and developing a general understanding of their behavior under various excitation patterns, great emphasis was placed on understanding the effect of noise and uncertainty in generic sets of data and assigning confidence intervals based on their projected fits. In order to understand the process of fitting models to data, several sets of data were generated based on a model plus random Gaussian noise to obfuscate the original model. Then, a model was derived analytically alongside a model generated using scientific computing code libraries and the two were compared. Finally, a confidence interval, or more accurately a "numerical budget", was created by sampling the covariance matrix generated by SciPy in the computer case, and the covariance matrix generated by inverting the fisher information matrix in the analytic case. Both covariance matrices were sampled by dotting a random vector and adding that value to the best fit parameters to simulate all possible deviations from the best fit model, and then highlighting the first (68%) and second (95%) sigma confidence intervals, as seen in 6.

3 Analyses

The first milestone accomplished during this project was learning, understanding, and modeling a two mirror cavity system both analytically and with computer simulations. Three equations were derived with a normalization factor to describe how electric fields behave inside a two mirror cavity, specifically focusing on their electric field strengths (in amplitudes) and their electric field phase change (in degrees), and seeing how these parameters evolve as a result of shifting some characteristic of the cavity in a process referred to as "tuning the cavity".

In order to simplify the analysis, the field amplitude and field phase were combined into a complex number whose absolute value represented the amplitude and complex phase represented the phase change in any incident laser light. The cavity was tuned by shifting the end mirror eight nanometers from left to right, treating the center as the point of resonance. The resonance of the cavity is defined as the length at which the laser interferes constructively between the two mirrors and destructively outside. In order for this to happen, the cavity length must be an integer number of wavelengths of the main laser.

The constants assumed for all cavity analyses were that both input and end mirrors have a power reflectivity, $r_i^2 = r_e^2 = 0.999$, that the transmissions of both input and end mirror were equal and conserved, $t_i = t_e = \sqrt{1 - |r_e|^2}$, the laser wavelength λ was 1064nm. The

laser light was phase modulated with a frequency of 24MHz, to a depth of 0.1 radians. This modulation was done to introduce smaller sidebands frequencies that are slightly off resonance whose behavior can be monitored to determine how close our desired carrier is to resonance. ϕ represents the "tuning" of the cavity. In this case, $\phi = \frac{2L\omega}{c}$ since we are specifically varying the cavity length L, but we could have chosen any other parameter to shift.

$$\frac{E_{cav}}{E_{in}} = \frac{t_i}{1 - r_i r_e e^{2i\phi}} * J_{0/1}(\Gamma) \tag{1}$$

Equation (1) models the electric fields inside the cavity, with a normalization factor of a bessel function of the first kind, $J_0(\Gamma)$ for the carrier wave and $J_1(\Gamma)$ for the upper and lower sidebands, which represents the electric field entering the cavity E_{in}.

$$\frac{E_{refl}}{E_{in}} = r_i - \frac{t_i^2 r_e e^{2i\phi}}{1 - r_i r_e e^{2i\phi}} * J_{0/1}(\Gamma) \tag{2}$$

Equation (2) models the electric fields reflected off the first mirror, with the same normalization factor of $J_0(\Gamma)$ for the carrier wave and $J_1(\Gamma)$ for the upper and lower sidebands as before.

$$\frac{E_{tran}}{E_{in}} = \frac{-t_i t_e e^{2i\phi}}{1 - r_i r_e e^{2i\phi}} * J_{0/1}(\Gamma) \tag{3}$$

Equation (3) models the electric fields transmitted entirely through the entire cavity, with the same normalization factor.

These three equations were used as the basis for the analytic description of how the electric fields behave in a cavity whose length is changing. A python script was developed to plug in all of our values and plot them to show how our carrier and sideband fields respond to changes in the cavity. In order to confirm the accuracy of these equations an interferometer simulation software named `FINESSE` was used to simulate the same two mirror system and corroborate its findings with the previous analysis. The results of reflected fields can be seen in Figures 1. The blue and green lines show an exact match between the analytic results and the simulation, and the orange lines show any differences between them, referred to as the residuals. The `FINESSE` code can be found in Appendix A.

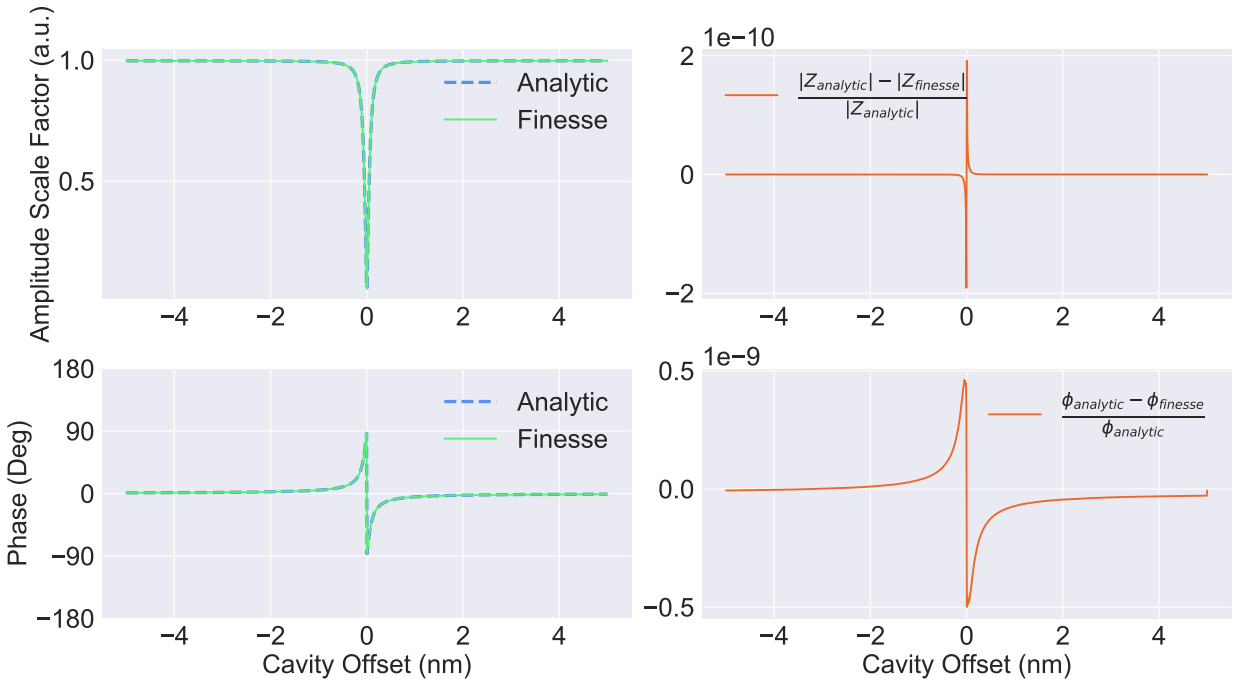

Figure 1: These four plots show the behavior of the carrier field reflected by the cavity (eq. (2)). The plots on the left side show the amplitude and phase change of fields. This plot shows an exact match between the analytic results and the simulation. The residuals agree with this conclusion.

In this project, we were most interested in locking the frequency of the laser to a set value to minimize our lasers from drifting off resonance. One of the main difficulties with using interferometers as gravitational wave detectors is that it is very difficult to have your laser frequency match the cavity resonance conditions exactly since the cavity parameters tend to drift. This drifting is due to random fluctuations, for example, small vibrations from the earth can change the length of the cavity, imperfections in the mirror coatings can alter the reflection coefficients, and imperfections in the laser crystal can excite unwanted harmonics and cause the frequency of the laser itself to wander. All of this make it almost impossible to lock onto a sensitive cavity since the cavity is only resonant for a very tiny range of frequencies.

The most common method of stabilizing the frequency of the laser is called the Pound-Drever-Hall technique which employs the use of a phase modulator to create upper and lower sidebands in the field of the laser whose purpose is to serve as "guards" for the carrier frequency from wandering too high or too low. If the laser is perfectly locked to the cavity, then these sidebands will reflect off the cavity. If the laser frequency is too high, then the upper sideband will not be reflected as before and this will trigger control systems to lower the laser frequency, and vice versa if the laser frequency is too low then the lower sideband will not be reflected as before and the control systems will raise the laser frequency. This negative feedback loop is an essential control system in locking a laser to a cavity.

The PDH technique is analytically derived in Appendix B of J. Driggers Thesis [7] to arrive at the following equations for the in-phase portion and quadrature-phase portions of the error signal. The sidebands reflect off the cavity and they are demodulated in order to arrive at the following equations for the amplitude of the error signal. If the phase of the local oscillator is set correctly, then the q-phase signal will disappear, leaving only the in-phase signal to serve as a source for the laser frequency control.

$$V_{refl}^{I} = \; J_0(\Gamma)\; J_1(\Gamma)\; \mathrm{Re}\big[r_{cav}(\omega) r_{cav}^{*}(\omega+\Omega) + r_{cav}^{*}(\omega) r_{cav}(\omega-\Omega)\big] \tag{4}$$

$$V_{refl}^{Q} = \; J_0(\Gamma)\; J_1(\Gamma)\; \mathrm{Im}\big[r_{cav}(\omega) r_{cav}^{*}(\omega+\Omega) - r_{cav}^{*}(\omega) r_{cav}(\omega-\Omega)\big] \tag{5}$$

After establishing and confirming simulation environments for electric fields in Fabry-Perot cavities, a comparison between 0 sideband and 5 sideband simulation was conducted. This was done in order to investigate how the analytic derivations may vary from the "true" result, since the PDH-signal equation assumes the existence of only one sideband, where in practice there may be several more whose contributions lessen the further they get from the carrier resonant point. The following plot shows the discrepancies between the 0 sideband and 5 sideband `FINESSE` simulations.

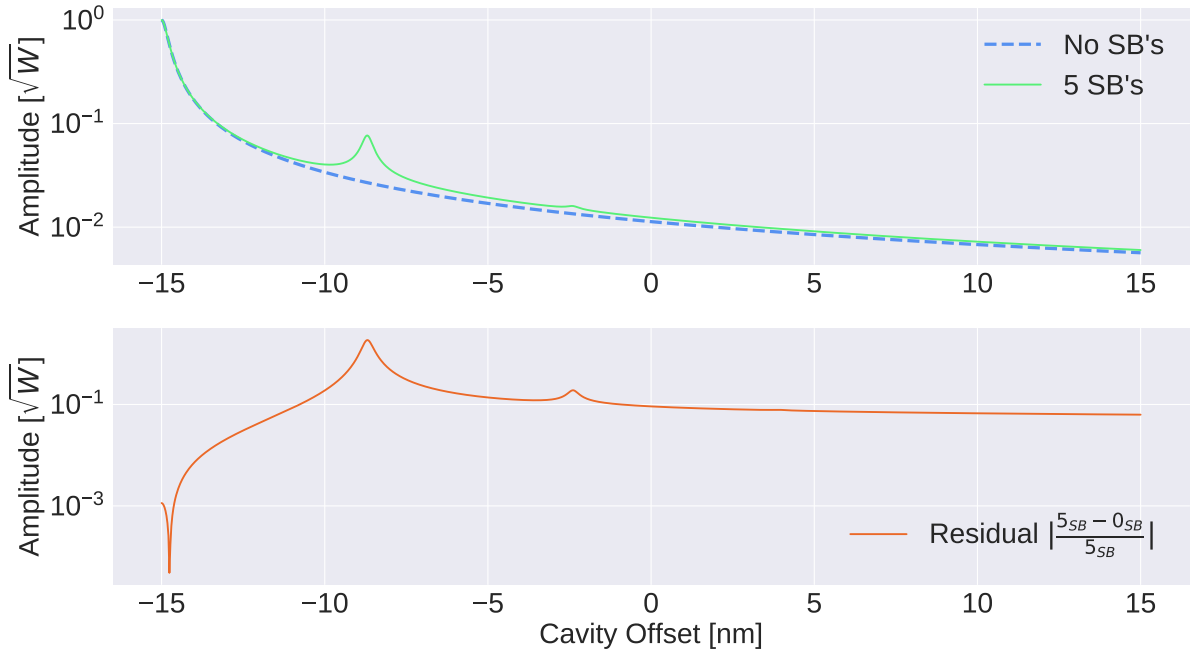

Figure 2: This plot shows the same 0 vs 5 sideband comparison as the previous plot, but instead shows the fields transmitted through the cavity. One can see the resonant frequencies that the sidebands respond to in the cavity, and that each sideband is separated by about 6nm worth of tuning in the cavity.

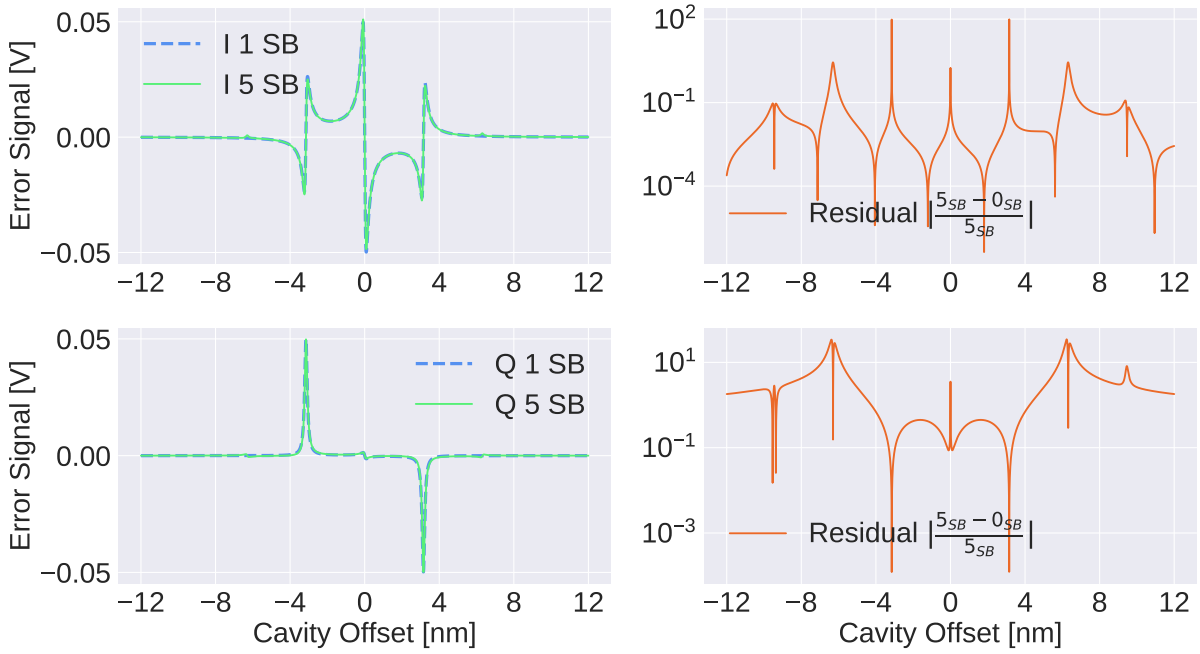

Figure 3: These four plots show the PDH error signal that determines the required mirror tuning in response to scanning the cavity length from -12 to +12 nm. This PDH signal is sampled from the light reflected off the cavity, and is identical from light transmitted through the cavity. In situ, the local oscillator would be phase shifted so that the quadrature phase (bottom plots) is pushed to zero, and then the in phase PDH signal is used to a drive a self-correcting servo on one cavity mirror.

After the sideband behaviors were analyzed and discussed, the project then moved on to characterize the affect of shot noise and length noise on the signal. For the next analysis, we introduced photon shot noise which is the uncertainty associated with the counting of photons. This project measured the shot noise as a function of the time elapsed while counting, since shot noise is fundamentally a Poisson-like distribution of photon counts measured at the photodiodes. A fast sweep results in a low number of counts and leads to shot noise dominating the signal, and a slow sweep leads to a high number of photon counts which reduces the uncertainty by a factor of $\sqrt{N}$ much like any other Poisson distribution. At this point in the project, we also added a few new important parameters regarding time such as the number of samples taken becoming a function of the time elapsed measuring (referred to as sweep time) and the sampling rate (≈100MHz).

$$\sigma_{shot} = \sqrt{\frac{\hbar\omega P_{laser}}{\tau_{sweep}}} = \sqrt{\frac{h\omega P_{laser}}{\tau_{sweep}}}$$

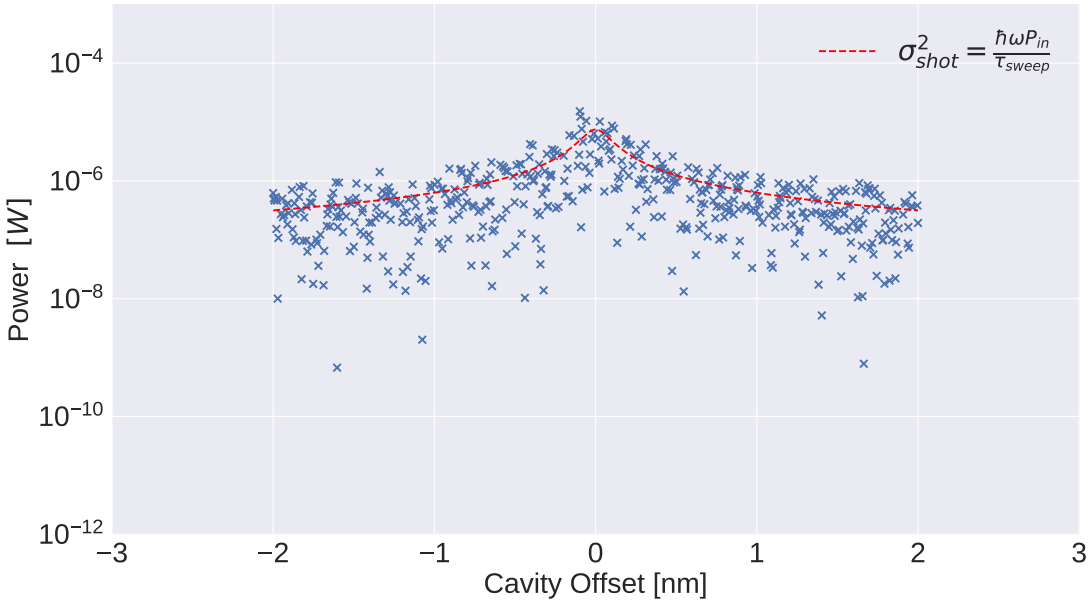

Figure 4: The randomly generated shot noise, in this case setting $\tau_{sweep} = 100\mu s$. The red curve represents the standard deviation of the expected shot noise, and this was used to sample a Gaussian distribution for N samples of shot noise for each data point in the simulated cavity transmitted power.

In addition to shot noise, we created simulations for another major source of noise known as length noise. Length noise is generally associated with the uncertainty in the true position of our servo motors during a cavity sweep, but can also arise from any other coupling mechanism that affects the relative distance of our mirrors. A realistic estimate for an amount of length noise we'd see in the lab is about a 0.03nm, for which the plot of the simulation can be seen below.

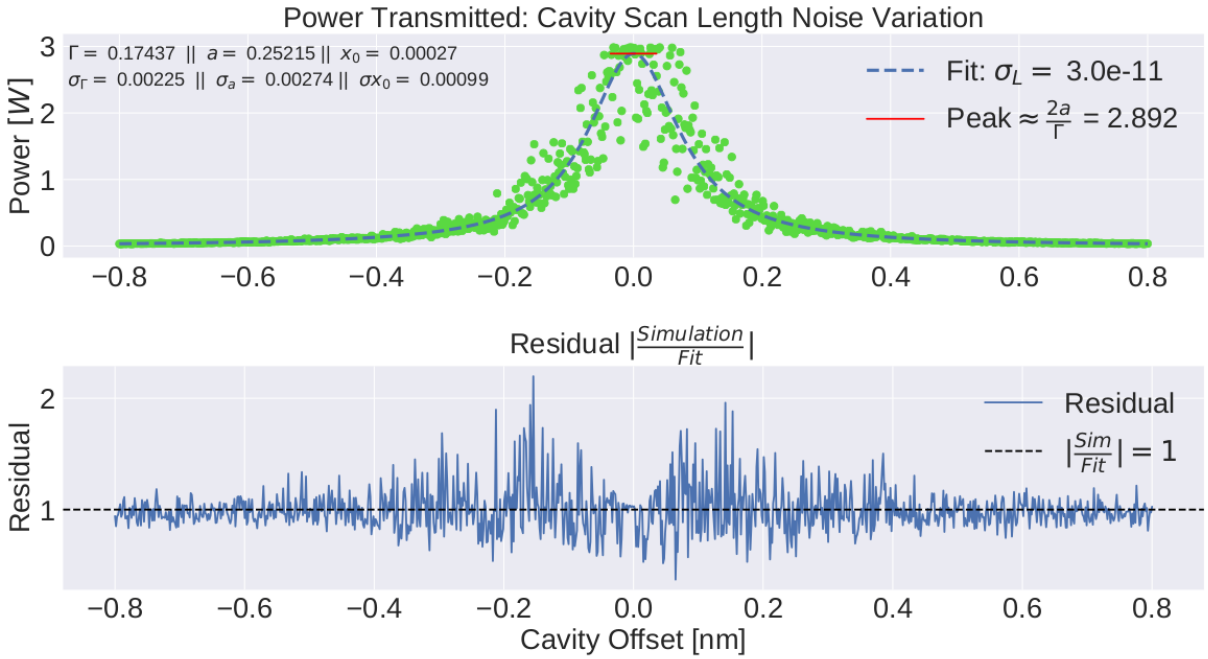

Figure 5: The randomly generated shot noise, in this case setting $\tau_{sweep} = 100\mu s$. The red curve represents the standard deviation of the expected shot noise, and this was used to sample a Gaussian distribution for N samples of shot noise for each data point in the simulated cavity transmitted power.

Developing mathematical models for sets of data is a critical part of any experimental process, and equally so for this project. In order to extract information from the data we simulate, the data must be scrutinized with a statistical lens which then leads to increased capacity to derive experimental parameters and assert their accuracy with specific levels of confidence. This can become very unwieldy when it comes to experiments with various equations, parameters, and models, thus the involvement of statistics in this project was taken in several steps.

First, a random set of data based on a linear model $y = mx + b$ was generated and then the values for m and b were determined concurrently. In one method, the data and each data point's uncertainty was plugged into the scientific computing package known as SciPy's `curve_fit()` algorithm, which returned two values of m and b with a two dimensional covariance matrix. The second method was more analytic and involved manually calculating a least squares sum, inverting the coefficient matrix and solving for the parameters, as well as constructing a fisher information matrix and inverting it to obtain the covariance matrix. These covariance matrices were then sampled using 10,000 random vectors and plotted to obtain a 1-σ and 2-σ confidence interval, as seen below.

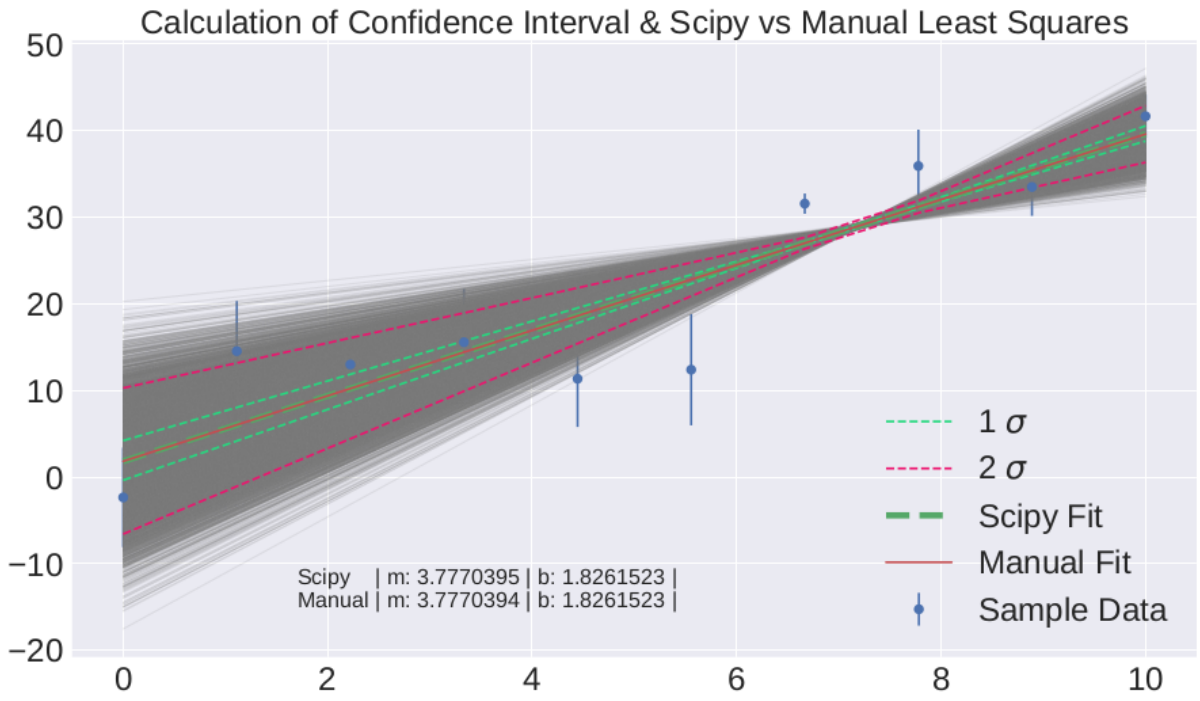

Figure 6: A set of data was generated by explicitly calculating $y = mx + b$ for a set of x-values, and for each data point a random amount of Gaussian noise was added and assigned an uncertainty. The manual fit was determined by calculating a least squares sum, and the SciPy fit was determined using SciPy's curve fitting algorithm. The 1-σ and 2-σ lines were determined by using a sorting algorithm on each set of y-values corresponding to a single x-value, and then taking the upper and lower 34 percentiles, and 95 percentiles.

The next round of practice was done on simulated data from `FINESSE`. The equation that describes the behavior of transmitted power through a Fabry-Perot cavity takes the form of Lorentzian, also known as the Cauchy Distribution, given by the equation:

$$\mathcal{L} = A * \frac{\frac{1}{2}\Gamma}{(x - x_0)^2 + (\frac{1}{2}\Gamma)^2}$$

This equation was used in conjunction with SciPy's `curve_fit()` algorithm to obtain the best fit parameter for x_0, Γ, and scaling factor A along with the 3x3 covariance matrix associated with these parameters. The same procedure for the determining the 1-σ and 2-σ was performed, although the SciPy fit had such low uncertainty that the first and second confidence intervals are directly overlaid onto the data signal, indicating that SciPy believes the Lorentzian fitting the data perfectly, which is what we expect given that the Lorentzian is the equation that governs the phenomenon of resonance.

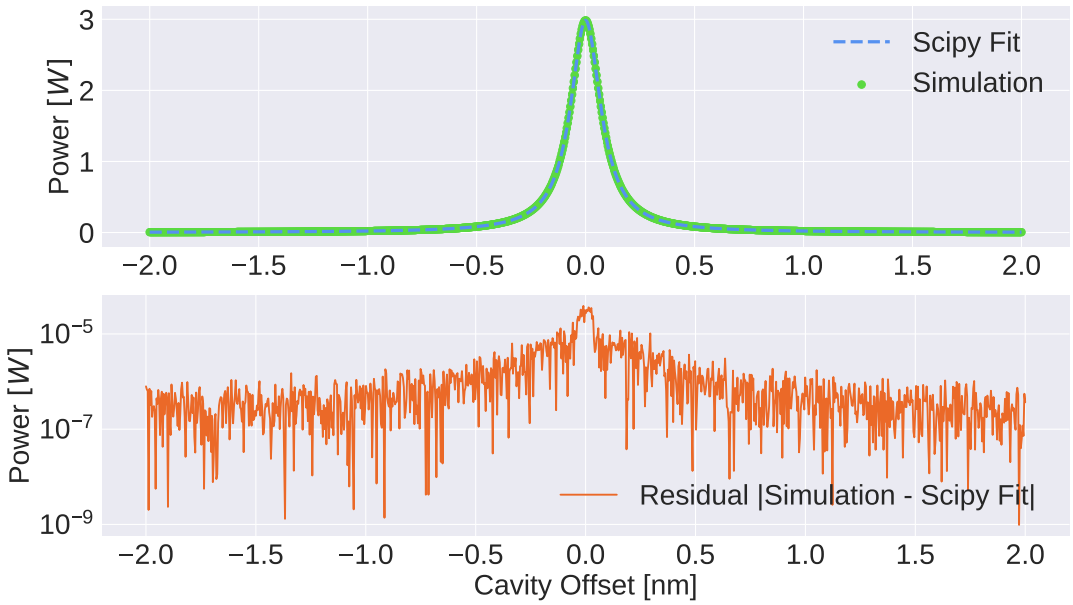

Figure 7: This plot shows the residual between the SciPy fit and the simulation, and with comparison to Figure 4 shows that the residual is on the same order of magnitude as the expected shot noise, indicating a close fit between the SciPy model and the data.

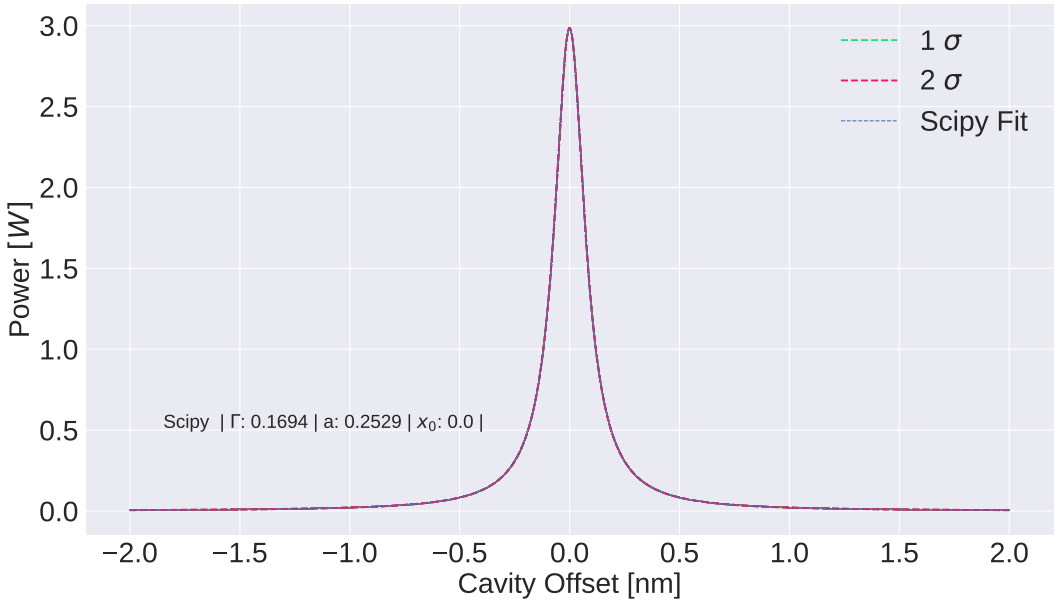

Figure 8: This plot shows the same procedure used to determine the first and second sigma confidence intervals for the linear fit, however the fit matches so well that the projected threshold for 68% and 95% are extremely small.

After having done all of these exercises in statistics and curve fitting, real data from an actual laser cavity at the Coating Thermal Noise Lab at Caltech was used to fit a Lorentzian. This data was taken on May 8th, 2019, by graduate student Anchal Gupta.

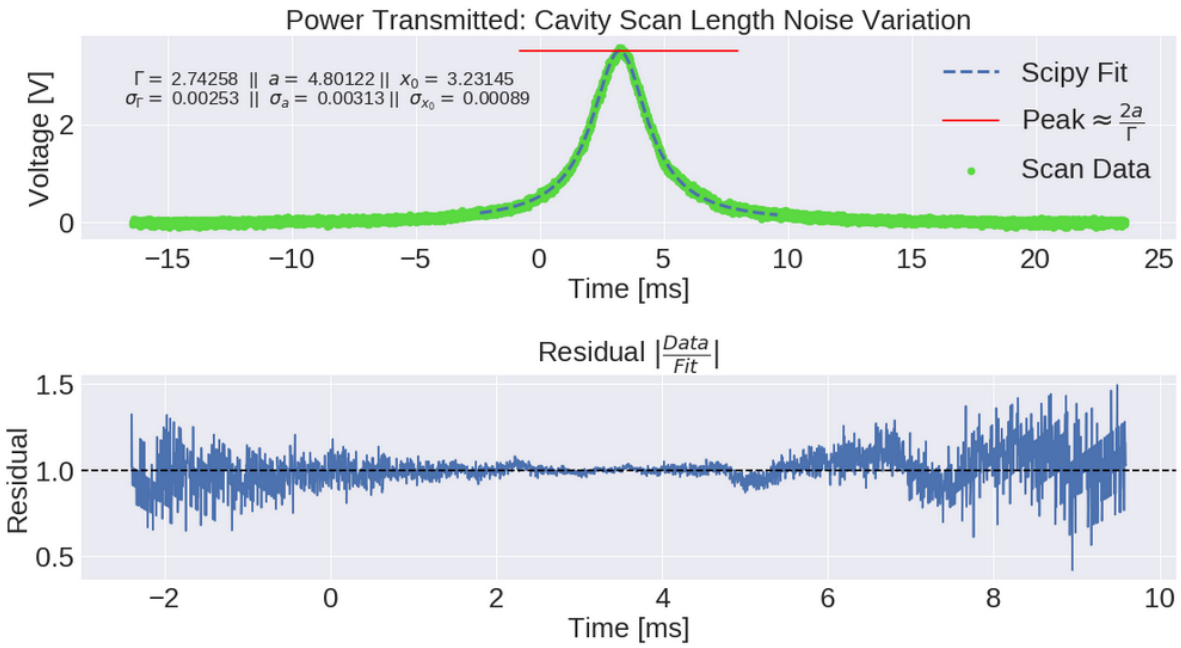

Figure 9: Real data from a cavity scan done in May. The three parameters represent the variables of the Lorentzian distribution- γ is the half-width half-maximum, a is the scale factor, and x_0 is the offset.

Finally, the project evolved from using traditional nonlinear regression fitting methods to a more modern technique known as Monte Carlo Markov Chain (MCMC) methods. By collecting all of our fitting variables for our model into a parameter space, we used python to simulate several hundreds of random "walkers" that would move around in parameter space based on a series of likelihoods. Each dimension of parameter space represented a variable in our fit, and then by allowing the walkers to move and then check how their goodness of fit compares between locations we arrived at new fits that highlighted the covariance between cavity parameters.

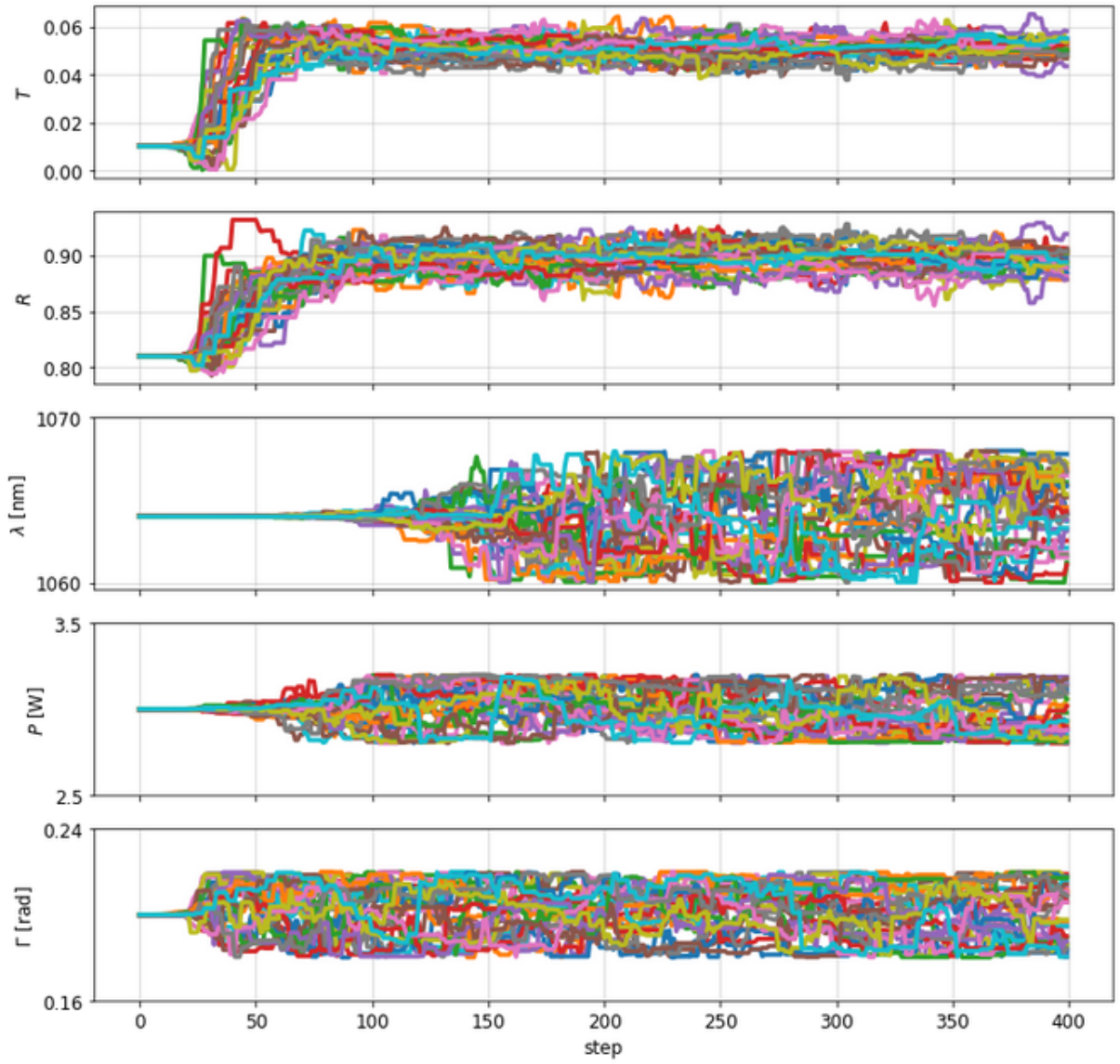

Figure 10: This plot shows 1000 walkers each taking 600 random steps trying to find the set of parameters with the best fit. $T = T_endT_input$ and $R = R_eR_input$ are cavity transmission/reflectivity parameters and converge relatively quickly, however the laser wavelength, laser power, and modulation depth do not converge at all.

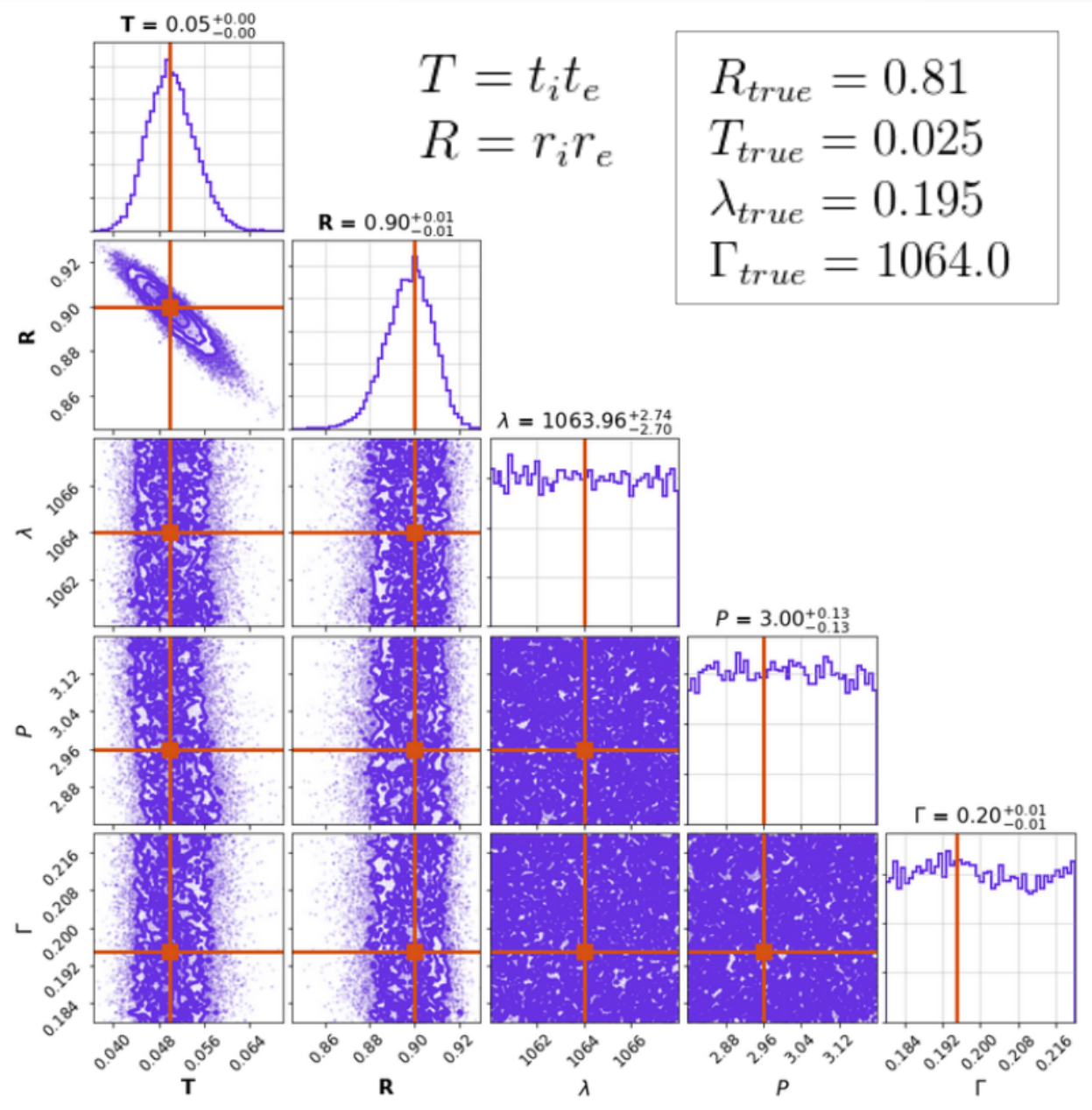

Figure 11: This plot shows the scatter plots of all parameters each walker ended on. The T vs R scatter plot shows a negative covariance plot which was what we expected based off the conservation law for reflection and transmissions.

4 Future Work

The immediate future work involves improving the MCMC fit done to simulation data by introducing a new likelihood function alongside a non-flat prior. Currently, the MCMC fit only judges each walker's step by the final result of the fit, rather than the step in each direction of parameter space. By introducing a likelihood function that nudges each walker in the direction of more optimal parameters, as well as including a prior distribution to give each walker a headstart, we can develop much more precise fits with lower margins of error.

References

[1] Siegel, Ethan. *"Ask Ethan: Why Don't Gravitational Waves Get Weaker Like The Gravitational Force Does?"* Forbes, Forbes Magazine, 2 Mar. 2019,

[2] LIGO Scientific Collaboration, *The Sensitivity of the Advanced LIGO Detectors at the Beginning of Gravitational Wave Astronomy*. Physical Review D 93.11 (2016)

[3] DeWitt, Cecile M. et al. *"An Expanded Version of the Remarks by R.P. Feynman on the Reality of Gravitational Waves".* Wright-Patterson Air Force Base (edition-open-access.de). 1957

[4] http://www.tapir.caltech.edu/~teviet/Waves/gwave_spectrum.html

[5] Chen, Chiang-Mei, James M. Nester, and Wei-Tou Ni. *"A brief history of gravitational wave research."* Chinese Journal of Physics 55.1 (2017): 142-169.

[6] Brown, Daniel David, Freise, Andreas. *"Python interface and tools for Finesse"*. 30 June 2017. Zenodo http://doi.org/10.5281/zenodo.821390

[7] Jennifer Driggers, *Noise Cancellation for Gravitational Wave Detectors.* PhD Thesis. California Institute of Technology, Pasadena, 2015. Appendix B

[8] B F Schutz, *Gravitational-wave sources*. Classical and Quantum Gravity Vol 13, 11A (1996).

A Finesse Code

This is the code used to create a virtual two mirror cavity.1

```
#our two mirror cavity
{laser}  n1 {modulator}  n3 |mirror1|  n4  :space2:  n5  |mirror2|  n6

# place lasers + modulators
l laser 1 0 n0       # 1 Watt, 0 Freq. Offset
s space0 0 1 n0 n1   # 0 meter space, required for modulator
mod modulator 24000k 0.1 1 pm 0 n1 n2  # 24MHz, 0.1 depth, 1 sideband
s space1 0 1 n2 n3   # 0 meter space, required for modulator

# place our mirrors
m mirror1 0.999 0.001 0 n3 n4
s space2 0.037 1 n4 n5
m mirror2 0.999 0.001 0 n5 n6
```

When analyzing the carrier and sideband fields at a certain location designated by N, these commands were supplied to Finesse.

```
# place amplitude detectors at location {N} (reflected, cavity, or transmitted)
ad AmpDetector 0 {N}
ad USBDetector 24000k {N}
ad LSBDetector 24000k {N}

# shift the mirror tuning, phi, by degrees denoted by S1 and S2.
# Since finesse only accepts degrees for phi,
# convert 5nm to degrees by multiplying 5nm by 360/1064.
xaxis mirror2 phi lin {S1} {S2} {Num}
yaxis lin abs:deg
```

When analyzing the Pound-Drever-Hall error signal, these commands were supplied to Finesse.

```
# place photodetectors to observe the sideband
# behavior to determine error signal
pd1 inphase 24000k 0 n3
pd1 quadphase 24000k 90 n3

# shift the mirror tuning, phi, by degrees denoted by S1 and S2.
# Since finesse only accepts degrees for phi, convert 5nm to degrees by
xaxis mirror2 phi lin {S1} {S2} {Num}
yaxis lin abs
```